ICWE14
June 21-26, 2015 | Porto Alegre - Brazil
14th INTERNATIONAL CONFERENCE ON WIND ENGINEERING

Wind tunnel tests on elongated rectangular plates under flutter motion: limit-cycle oscillations and preliminary energy harvesting considerations

Luca Pigolotti [1], Claudio Mannini[1], Gianni Bartoli[1], Klaus Thiele[2]
[1]CRIACIV/Department of Civil and Environmental Engineering, Università degli Studi di Firenze, Italy
[2]Institut of Steel Structures, Technische Universität Braunschweig, Germany
email: luca.pigolotti@dicea.unifi.it, claudio.mannini@dicea.unifi.it, gianni.bartoli@unifi.it, k.thiele@is.tu-braunschweig.de

ABSTRACT: Energy harvesting from aeroelastic instabilities is a recent solution to provide alternative power generators. In particular, the two-degrees-of-freedom classical flutter involves relevant amounts of energy that can be extracted to generate electricity through a suitable conversion apparatus. To provide effective generators, stable steady-state oscillations after the instability onset are required. The problem involves several parameters and an important open issue is the basic post-critical dynamics of flutter on which the research is evolving nowadays. In the present study, the parametric space is investigated in order to understand its main features. The critical condition and the role of some parameters on the power efficiency were preliminary explored with linear analyses. Wind tunnel tests were conducted to experimentally validate the numerical results and to focus the investigations on the system behavior after the instability threshold. The energy generation is simulated through additional damping on the degree of freedom in which the conversion apparatus is assumed to act. According to the obtained results, optimal powering systems based on flutter should mainly operate at low reduced flow velocities. Furthermore, the position of the mass and elastic centres can be used as tuning parameters of the operative range and they should be moved downstream the midchord of the cross section to anticipate the instability onset and to enhance the powering performance.

KEY WORDS: Flutter, Post-critical Dynamics, Flat Plate, Wind Tunnel Tests, Power Efficiency, Parametric Analysis.

1 INTRODUCTION

In the common practice of wind and aeronautical engineering, dynamic fluid-structure interaction is considered as a dangerous phenomenon and the design of structures prone to flow-induced vibrations usually focuses on limiting any excursion in the post-critical range. In particular, several aeroelastic phenomena (see for example [1] for a general review) can arise when slender structures are excited by the wind flow to produce cross-flow, self-induced aerodynamic loads with important nonlinear effects, sometimes leading to catastrophes [2]. These kinds of dynamic instability can exhibit limited Limit Cycle of Oscillation (LCO), as in case of Vortex-Induced Vibrations (VIV), or unrestricted LCO with the flow velocity after a critical threshold, as in case of galloping, stall flutter and classical flutter. The latter usually features rapidly increasing LCO, where the mechanism for the energy transfer between airstream and structure relies on elastic and/or aerodynamic coupling between two modes, mainly bending (or heaving) and torsional (or pitching) modes, as well as a phase lag between a displacement and its aerodynamic reaction (*e.g.* [3, 4]). In addition, nonlinear aerodynamic reaction to the motion of the structure due to pitching excursions beyond the stall angle and other nonlinear effects of mechanical nature, such as internal material hysteresis and friction, can dissipate energy and modify the system response as well (*e.g.* [5]).

From a different perspective, recent studies on alternative energy production showed the possibility of exploiting fluid-elastic instabilities to capture the flow energy and generate electricity. Coupling the mechanical system with a suitable energy conversion apparatus, mainly based on electromagnetic induction and piezoelectric effect (*e.g.* [6]), usable power is available during steady-state oscillations. According to this principle, some authors have preliminary explored the capability of aero-/hydro-elastic generators, mainly focusing on elastically suspended rigid bodies that rely on: VIV [7]; transverse [8, 9], torsional [8, 10] and wake [11] galloping; flapping [12, 13, 14, 15, 16, 17, 18] and fluttering [19] wings. Continuous flexible bodies were also investigated [20, 21, 22, 23, 24], especially exploiting internal coupling effects between structure, piezo patches and electric circuit [25, 26]. The most promising results were obtained for two-Degree-of-Freedom (2-DoF) fluttering systems, though they often involve externally driven pitching motion and specific airfoil-shaped cross sections. Nevertheless, research on power generation from flow-induced vibrations is still a recent topic and most of the previous studies were essentially limited to theoretical and numerical analyses.

The present work focuses on wind-induced, 2-DoF classical flutter, in particular from the experimental point of view. For energy harvesting purposes, the system needs to perform self-sustained oscillations beyond the instability threshold to

effectively produce power and the post-critical behaviour becomes of crucial importance. The main issues are the critical reduced velocity, at which instability arises, and the features of the LCOs. Despite the many available studies on dynamic stall flutter mechanism (*e.g.* [27, 28, 29, 30, 31]), due to the importance for wings operating at high angles of attack (rotor blades of wind turbines and helicopters), research on post-critical classical flutter is not extensive. The common interest for conventional civil/aeronautical structures is devoted just to the prediction of the linear instability threshold (*e.g.* [32]) and the available predictive models mainly concern dynamic stall (*e.g.* [33, 34, 35]). In addition, there are some not well-known problems about the physical sources of nonlinearity, because the literature studies often focused on classical flutter LCOs under specific nonlinear mechanical boundary conditions (*e.g.* [36, 37, 38]). Hence, further research is required on reliable aeroelastic models and experimental setups for large oscillations to adequately face the post-critical behaviour in case of classical flutter.

Linear aeroelastic models were used herein to parametrically explore the critical conditions. Wind tunnel tests were conducted to observe the aeroelastic behaviour of an aluminium sectional model, with a 15:1 (width-to-depth) cross section, chosen to exploit previous results [39, 40] and to allow feasible experiments according to the characteristics of the available wind tunnel facility. A coil-spring-based aeroelastic rig was developed to explore the effect on the flutter instability of some dominant parameters, mainly the positions of the stiffness and mass centres (c.e. and c.m. in Figure 1a). In the configurations tested (Figure 1b), the total participating masses ranged between 13.4 and 15.4 kg, the oscillation frequencies were around 2 Hz, while the investigated flow speeds were in the range 7-18 m/s. An electromagnetic device was used to increase the damping of the system up to about 5.7%, simulating also the energy extraction process [6].

2 METHODOLOGY

2.1 Linear aeroelastic models

According to the available linear models for the self-excited loads, Theodorsen's model [3] derives from potential flow theory applied on a theoretical flat plate and is taken here as reference for comparisons. Nevertheless, the investigated width-to-depth ratio of the cross-section is 15:1 and the flat plate assumption is not fully suitable. Thus, the Scanlan's model [32] is considered, exploiting the experimental flutter derivatives reported in [40], to perform more appropriate predictions for this case study.

The 2-DoF flutter problem is sketched in Figure 1a and the governing equations are reported in nondimensional form throughout Eqs. (1, 2, 3), assuming $\eta(t) = \eta^* e^{i2\pi nt}$ and $\alpha(t) = \alpha^* e^{i(2\pi nt+\phi^*)}$ where n and ϕ^* are the frequency of oscillation and phase difference at flutter:

$$\begin{cases} \mu\left\{\left[\left(1+ig_\eta\right)\frac{X}{\gamma_n^2}-1\right]\frac{\eta(t)}{B}-x_m\alpha(t)\right\} = \bar{L}_{\eta,j}(\eta,\alpha,K,x_e,t) \\ \mu r_\alpha^2\left\{[(1+ig_{\alpha0})X-1]\alpha(t)-\frac{x_m}{r_\alpha^2}\frac{\eta(t)}{B}\right\} = \bar{M}_{\alpha,j}(\eta,\alpha,K,x_e,t) \end{cases}; \tag{1}$$

$$\begin{aligned} \bar{L}_{\eta,S}(t) &= [H_4^*(K)+iH_1^*(K)]\frac{\eta(t)}{B}+[H_3^*(K)+iH_2^*(K)]\alpha(t)\,; \\ \bar{M}_{\alpha,S}(t) &= [A_4^*(K)+iA_1^*(K)]\frac{\eta(t)}{B}+[A_3^*(K)+iA_2^*(K)]\alpha(t)\,; \end{aligned} \tag{2}$$

$$\begin{aligned} \bar{L}_{\eta,T}(t) &= -\left[-\frac{\pi}{2}+iC_L'\frac{C(k)}{K}\right]\frac{\eta(t)}{B}-\left\{\left[\frac{\pi x_e}{2}+C_L'\frac{C(k)}{K^2}\right]+i\left[\frac{\pi}{2K}+C_L'\frac{C(k)}{K}\left(\frac{1}{4}-x_e\right)\right]\right\}\alpha(t)\,; \\ \bar{M}_{\alpha,T}(t) &= \left[-\frac{\pi x_e}{2}+iC_M'\frac{C(k)}{K}\right]\frac{\eta(t)}{B}+\left\{\left[\pi\left(\frac{1}{64}+\frac{x_e^2}{2}\right)+C_M'\frac{C(k)}{K^2}\right]+i\left[-\frac{\pi}{2K}\left(\frac{1}{4}-x_e\right)+C_M'\frac{C(k)}{K}\left(\frac{1}{4}-x_e\right)\right]\right\}\alpha(t). \end{aligned} \tag{3}$$

The heaving amplitude is normalized by the chord (width) $B = 2b$ and the length L of the model is used to obtain aerodynamic and mechanical quantities per unit span. Moreover, g_η and $g_{\alpha0}$ are the coefficients of rate-independent damping for heaving and pitching modes and are used instead of the ratio-to-critical damping $\xi_\eta = \xi_{\eta0} + \xi_{\eta E}$ and $\xi_{\alpha0}$:

$$\begin{aligned} g_\eta &= 2\xi_\eta\,\omega/\omega_{\eta0} = g_{\eta0}+g_{\eta E}\,; \\ g_{\alpha0} &= 2\xi_{\alpha0}\,\omega/\omega_{\alpha0}\,; \end{aligned} \tag{4}$$

where $\omega_{\eta0} = 2\pi n_{\eta0}$ and $\omega_{\alpha0} = 2\pi n_{\alpha0}$ are the circular frequencies of the modes in still air. Concerning the notation of ξ_η and g_η, the subscript "0" stands for the mechanical damping, while "E" for the external damping that can be varied with the electromagnetic dampers. In Eq. (4), $\omega_{\eta0}$ and $\omega_{\alpha0}$ are assumed (and experimentally verified) to not vary with the external heaving damping. The parameters C_L' and C_M' are the slopes of the lift and moment aerodynamic coefficients, that for a flat plate are equal respectively to 2π and $2\pi\,(1/4+x_e)$, while $C(k)$ is Theodorsen's circulatory function [3] depending on $k = \omega b/U$. The dimensionless aerodynamic derivatives $H_i^*(K)$ and $A_i^*(K)$ ($i = 1, 2, 3, 4$), which depend on $K = 2k$, required corrections as compared to those experimentally obtained in [40], hereinafter called $H_{i,0}^*(K)$ and $A_{i,0}^*(K)$, to account for eccentricity of the elastic centre with respect to the midchord. Moreover, experimental flutter derivatives were measured up to reduced velocities

($U_{R\alpha}$ in Eq. (6)) lower than those achieved in the present tests. Thus, after an interpolation with a 3rd-order polynomial and an extrapolation in the range of interest, they were assumed to follow the relationships in Eq. (5):

$$
\begin{aligned}
&H_1^*(K) = H_{1,0}^*(K)\ ;\\
&H_2^*(K) = H_{2,0}^*(K) - x_e H_1^*(K)\ ;\\
&H_3^*(K) = H_{3,0}^*(K) - x_e H_4^*(K)\ ;\\
&H_4^*(K) = H_{4,0}^*(K)\ ;\\
&A_1^*(K) = A_{1,0}^*(K)[1+4x_e]\ ;\\
&A_2^*(K) = \left[A_{2,0}^*(K) + \frac{\pi}{8K}\right][1+4x_e] - \frac{\pi}{8K} - x_e A_1^*(K) + \frac{\pi x_e}{2K}\ ;\\
&A_3^*(K) = \left[A_{3,0}^*(K) - \frac{\pi}{64}\right][1+4x_e] + \frac{\pi}{64} - x_e A_4^*(K)\ .\\
&A_4^*(K) = A_{4,0}^*(K)[1+4x_e] - \frac{\pi x_e}{2}\ .
\end{aligned}
\tag{5}
$$

The main assumption behind these equations is that circulatory, apparent inertias and centrifugal terms [3] contribute to the aerodynamic derivatives according to the same structure as that deduced from Theodorsen's theory.

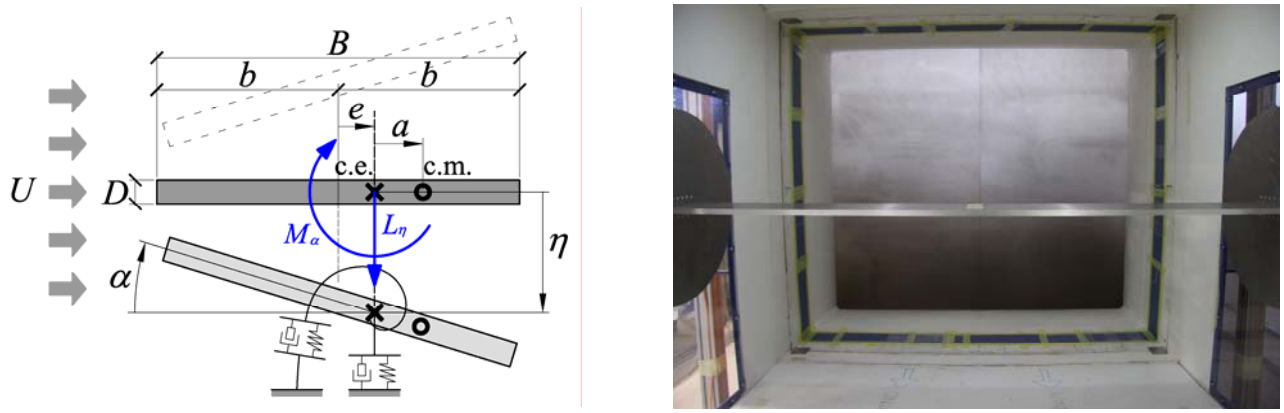

(a) (b)

Figure 1. Sketch of the two-dimensional flutter problem (a), in which Scanlan's convention is followed. Internal view of the test section with the model installed (b).

Table 1. Domains of the parameters tested through numerical investigations, with $B = 0.15$ m and $n_{\alpha 0} = 2.28$ Hz. Δ indicates the discretization step of the generic interval [·, ·] while {·; ·; ·; ...} denotes set of values.

Configuration	ξ_η [%]	ξ_α [%]	x_e [-]	μ [-]	x_m [-]	r_α [-]	γ_h [-]
reference	0.09	0.17	0.00	948.8	0.00	0.84	1.28
x-0-0-0-0-0-0	[0.09, 40] Δ=2	〃	〃	〃	〃	〃	〃
0-**x**-0-0-0-0-0	〃	[0.17, 4] Δ=0.2	〃	〃	〃	〃	〃
0-0-**x**-0-0-0-0	〃	〃	[-0.5, 0.5] Δ=0.05	〃	〃	〃	〃
0-0-0-**x**-0-0-0	〃	〃	〃	[628.3, 1256.6] Δ=31.4	〃	〃	〃
0-0-0-0-**x**-0-0	〃	〃	〃	〃	[-0.5, 0.5] Δ=0.05	〃	〃
0-0-0-0-0-**x**-0	〃	〃	〃	〃	〃	[-0.5, 0.5] Δ=0.05	〃
0-0-0-0-0-0-**x**	〃	〃	〃	〃	〃	〃	[1, 3] Δ=0.1
x-0-**x**-0-0-0-0	[0.09, 40] Δ=2	〃	{-0.1; 0.1; 0.2; 0.3; 0.4}	〃	〃	〃	〃
x-0-0-0-**x**-0-0	[0.09, 40] Δ=2	〃	〃	〃	{0.05; 0.15; 0.25; 0.35; 0.45}	〃	〃

The other dimensionless parameters that play a role in the flutter problem are: x_e, position of the centre of elasticity; μ, ratio between the masses of model and moved air; x_m, position of centre of mass; r_α, radius of polar inertia; γ_n, frequency ratio in still air of the uncoupled modes; X, unknown nondimensional frequency of flutter; $U_{R\alpha}$, reduced flow velocity:

$$x_e = \frac{e}{B}; \quad \mu = \frac{2M_\eta/L}{\rho B^2}; \quad x_m = \frac{a}{B}; \quad r_\alpha = \sqrt{I_\alpha/M_\eta B^2}; \quad \gamma_n = \frac{n_{\alpha 0}}{n_{\eta 0}}; \quad X = \left(\frac{n_{\alpha 0}}{n}\right)^2; \quad U_{R\alpha} = \frac{U}{n_{\alpha 0} B};, \tag{6}$$

2.2 Experimental setup

The experimental campaign was conducted in the Eiffel-type (open-return), boundary layer wind tunnel of the Stahlbau Institut, of TU in Braunschweig, Germany (Figure 2). The geometry of the test section is 1.40×1.20 m^2 (width×height) and the 55 kW fan, placed at the outlet, allows to vary the flow speeds in the range 2-25 m/s through an inverter. The present tests were conducted in smooth flow conditions with a free-stream turbulence intensity of about 1%.

The aeroelastic setup (Figure 2), arranged immediately downstream the inlet, was supported by an independent aluminium structure, externally enveloping the test section. Four coil springs (with an individual nominal stiffness of 220 N/m and a maximum elongation of 833 mm) and two analog laser displacement transducers (with an operative range of 50-300 mm and a sampling frequency of 1000 Hz) were installed at both ends of the model to observe the pitching (α) and heaving (η) motion. The damping of the heaving motion was controlled by an electromagnetic system, shown in Figure 2: setting the current intensity in a pair of electromagnets (with a nominal power of 15 W corresponding to a force of about 2800 N on a 9 mm iron plate in contact) at a small face-to-face distance, the magnetic field produced eddy currents in a copper/aluminium plate connected to the oscillating system and moving in the gap and thus a damping force.

Figure 2. View of the wind tunnel facility from the inlet side (top) and detail of the aeroelastic setup, showing the measuring apparatus and electromagnetic dampers (bottom).

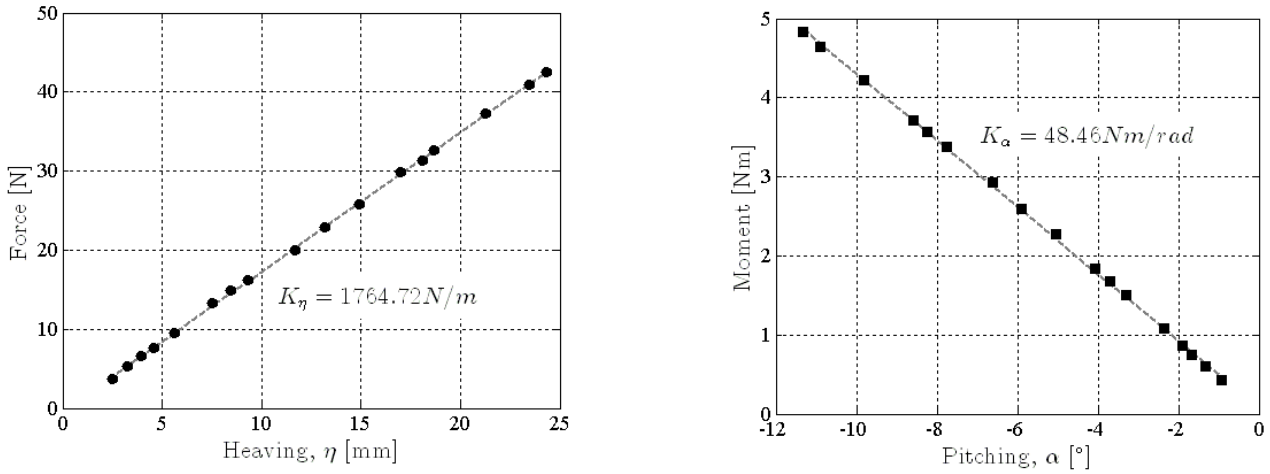

Figure 3. Example of the mechanical characteristics of the aeroelastic setup: heaving (left) and pitching (right) stiffness. The intrinsic geometrical nonlinearity of the setup in the pitching degree of freedom is negligible in the test range.

Table 2. Parameters of the configurations tested during the experimental campaign.

Configuration	ρ [kg/m^3]	M_η [kg]	I_α [kg·m^2]	S_α [kg·m]	$n_{\eta 0}$ [Hz]	$n_{\alpha 0}$ [Hz]	ξ_η [%]	ξ_α [%]	x_e [-]	μ [-]	x_m [-]	r_α [-]	γ_n [-]
#1	1.19	13.404	0.2107	0.047	1.839	2.387	0.09	0.20	0.00	831.9	0.025	0.836	1.298
#2	〃	〃	〃	〃	〃	〃	0.93	〃	〃	832.5	〃	〃	〃
#3	〃	15.364	0.2521	0.079	1.706	2.207	0.05	0.13	〃	953.8	0.035	0.854	1.294
#4	1.20	〃	〃	〃	〃	〃	0.86	〃	〃	947.5	〃	〃	〃
#5	〃	〃	〃	〃	〃	〃	〃	〃	〃	951.3	〃	〃	〃
#6	1.19	〃	〃	〃	〃	〃	2.57	〃	〃	953.2	〃	〃	〃
#7	1.20	〃	0.2439	0.306	〃	2.244	0.11	0.17	〃	947.5	0.135	0.840	1.315
#8	〃	〃	〃	〃	〃	〃	2.01	〃	〃	〃	〃	〃	〃
#9	〃	〃	〃	〃	〃	〃	3.08	〃	〃	〃	〃	〃	〃
#10	1.19	〃	0.2438	0.130	〃	〃	0.07	〃	〃	953.8	0.055	〃	1.316
#11	1.20	〃	〃	〃	〃	〃	3.11	〃	〃	945.0	〃	〃	〃
#12	1.19	〃	〃	〃	〃	〃	5.67	〃	〃	956.9	〃	〃	〃
#13	〃	〃	〃	0.185	〃	2.357	0.08	0.21	〃	956.9	0.080	〃	1.382
#14	〃	〃	〃	〃	〃	〃	5.40	〃	〃	956.9	〃	〃	〃
#15	1.17	14.822	0.2308	0.073	1.720	2.172	0.05	0.17	〃	935.6	0.035	0.832	1.263
#16	1.19	〃	〃	〃	〃	〃	〃	〃	〃	925.5	〃	〃	〃
#17	1.17	〃	〃	〃	〃	〃	5.66	〃	〃	941.8	〃	〃	〃
#18	1.19	〃	〃	〃	〃	〃	〃	〃	〃	926.1	〃	〃	〃
#19	〃	14.850	0.2386	0.092	1.718	2.136	0.07	0.14	-0.10	926.8	0.040	0.845	1.243
#20	〃	〃	〃	〃	〃	〃	〃	〃	〃	〃	〃	〃	〃
#21	〃	〃	0.2352	0.029	〃	2.151	〃	0.15	0.10	〃	0.015	0.839	1.252
#22	〃	〃	〃	〃	〃	〃	4.95	〃	〃	924.3	〃	〃	〃

The aluminium model, shown in Figure 1b, has a rectangular cross section with sharp edges and is 150 mm wide (B), 10 mm deep (D) and 1200 mm long (L); the smaller dimension D is the one facing the wind. The ad-hoc designed system to connect the model ends to the spring suspension also allowed to vary the position of the elastic centre. Circular aluminium end-plates, 400 mm large and 2 mm thick, were provided to ensure time-averaged bi-dimensional flow conditions. Additional masses were attached to the suspension system to shift the mass centre position. The along-wind motion was suppressed connecting cables to the model ends, close to the internal walls of the test section, and verifying that the variations of the vertical and torsional stiffness were small. The operative Reynolds number was in the range 70,000-180,000 ($Re = UB/\nu$, with $\nu = 0.15$ cm^2/s) and the mean flow speed was measured by a Pitot tube installed downstream the model and corrected through known flow maps to infer the velocity at the model centreline. The maximum blockage ratio was about 2.4%, reached at $\alpha \approx 14°$.

The stiffness linearity of the aeroelastic setup, in both the pitching and heaving degrees of freedom, were verified through static tests (Figure 3), measuring static displacement for different known loads. The participating inertia in the heaving and pitching motions, M_η and I_α, were calculated from the previously estimated stiffness and the corresponding frequency of oscillation in still air. Dynamic tests, in which the frequencies were measured for different additional inertias, confirmed the results. Moreover, for each configuration several free decay tests were performed in still air for different initial conditions, in order to evaluate the natural frequencies of oscillation ($n_{\eta 0}$, $n_{\alpha 0}$) and the structural ratio-to-critical damping coefficients

($\xi_{\eta 0} \approx 0.07\%$, $\xi_{\alpha 0} \approx 0.17\%$). Higher levels of ξ_η were reached through the electromagnetic system, up to a value of 5.67%. The static unbalance, S_α, was estimated by measuring the frequencies of oscillations of the system during coupled pitching-heaving motion [4]. Table 2 summarizes the governing parameters of the experimental system.

3 RESULTS AND DISCUSSIONS

3.1 Parametric linear analyses

In general, the linear analyses confirmed the expected difference between Scanlan's and Theodorsen's models, due to the 15:1 rectangular cross-section as compared to the hypothesis of flat plate. In particular, observing Figure 4, Theodorsen's model usually overestimates both the critical reduced velocity and the unknown dimensionless flutter frequency.

Figure 4 shows that both the critical reduced velocity and X always increase with the parameters μ, γ_n and $\xi_{\alpha 0}$. In the perspective of flutter-based generators, these two parameters have to be as low as possible in order to develop efficient powering systems, as explained by Eq. 7 in section §3.3, in which the main parameter for the efficiency is $U_{R\alpha}$ that appears in the denominator with a power of three. Furthermore, the ratio between the natural frequencies of the structural modes involved in the instability plays a key role and has to be close to 1. This condition implies a fast coupling and energy exchange between the modes, fostering the flutter motion at low $U_{R\alpha}$. In this way, also the unknown nondimensional frequency of flutter, X, is close to 1, thus it produces small effects on the energy performance in comparison to those ones of $U_{R\alpha}$.

The damping in the pitching DoF has to be exceeded by the negative aerodynamic damping to give rise to the instability and therefore the former should be as small as possible. By contrast, the polar inertia parameter r_α plays a particular role as it increases the critical reduced velocity while decreases the unknown dimensionless flutter frequency so that, according to Eq. 7, its effect on the powering efficiency is not immediately quantifiable.

Key parameters for lowering the critical reduced velocity are the position of elastic and mass centres. Designing systems with large eccentricity downstream the midchord of the cross section entails significant reduction of $U_{R\alpha}$. In Figure 4, decrements above 25% were simply achieved moving the elastic centre to the downstream quarter-chord position. A decrease of the critical reduced velocity was also obtained moving the mass centre toward the trailing edge. In particular, observing the predictions of Theodosen's model in Figure 4, which can be considered representative of width-to-depth ratios above 20:1 [40], a local minimum of $U_{R\alpha}$ occurs around $x_m = 0.2$. By contrast, X increases with both x_e and x_m and can slightly affect the energy performance, especially due to the marked dependence on the latter.

The power conversion process extracts energy form the fluid-structure system inducing a proportional damping into the system. Thus, the understanding of the system response to increments of the heaving damping is crucial, assuming that the energy convertion is performed only in the heaving DoF. Generally, the effect of damping on aeroelastic phenomena is to limit the instability. This is confirmed by Figure 4 that reports the evolutions of $U_{R\alpha}$ and X with the ratio-to-critical heaving damping coefficient ξ_η. Also in case of eccentricity of the elastic centre (right-hand side of Figure 5), which are particularly efficient configurations to reduce the critical velocity, an increase of ξ_η implies flutter stabilization with negative consequences for energy harvesting purposes. By contrast, for configurations with positive eccentricity of the mass centre (left-hand side of Figure 5), a significant increase of heaving damping produces small increments of $U_{R\alpha}$ but considerable reduction of X. In case of relevant positive mass eccentricity, saturation of these flutter parameters is achieved for values of ξ_η beyond 20-25%, therefore higher levels of power production are supposed to not considerably affect the system dynamics. In case of small eccentricity of the mass centre ($x_m = 0.05$), both Scanlan's and Thodersen's models exhibit a local minimum of the critical reduced velocity for values of ξ_η around 15-20%.

To sum up, a candidate flutter-based generator should feature low mass ratio and polar inertia, structural modes with close frequency and low torsional damping. Then, the position of the elastic and mass centres can be designed to tune the operative range of the system and the power output, controlled by the level of additional heaving damping.

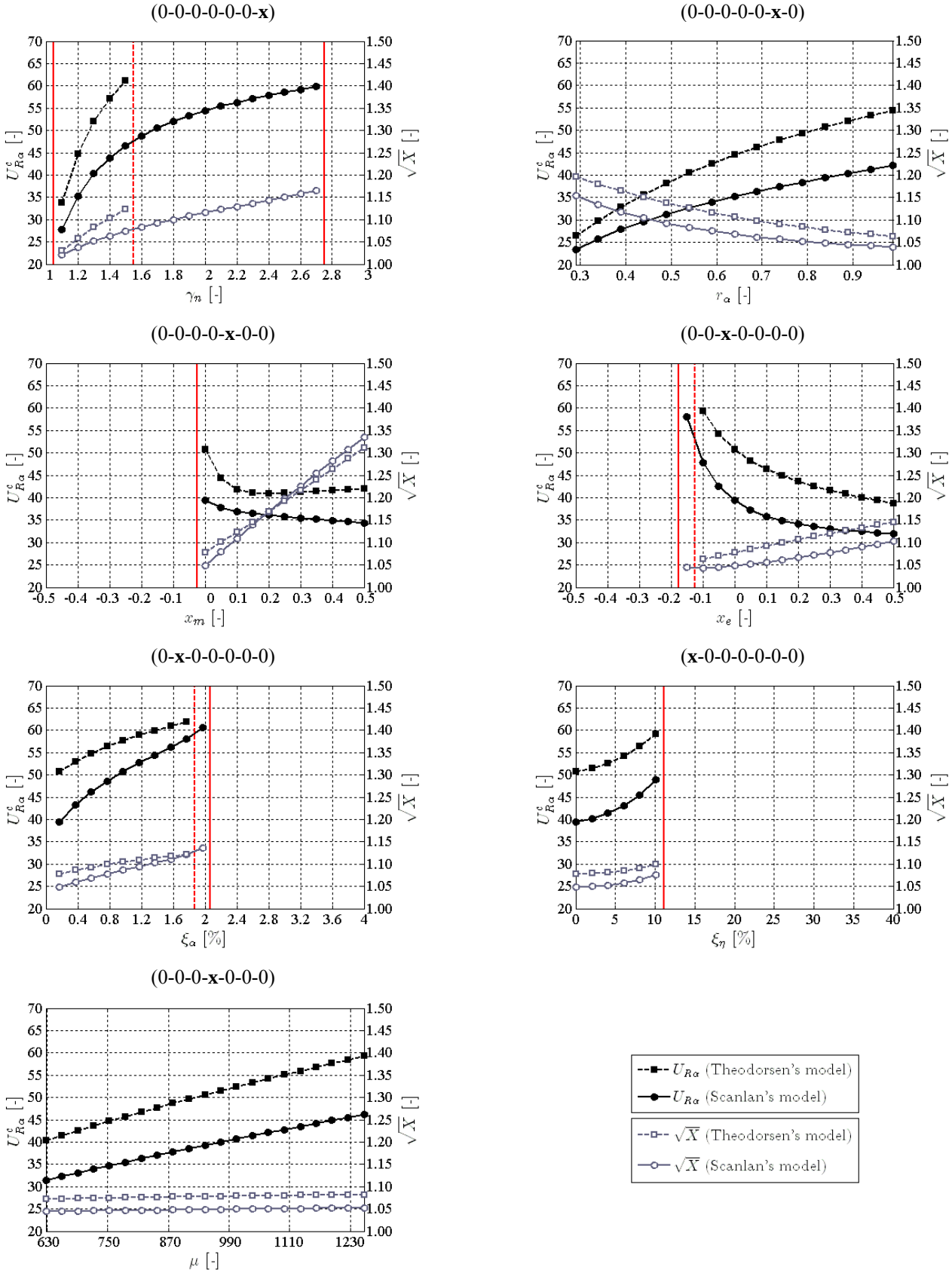

Figure 4. Results of the linear analyses, obtained varying one parameter by one according to Table 1, in terms of critical reduced velocity ($U^c_{R\alpha}$) and ratio of pitching still-air frequency to flutter frequency ($\sqrt{X}$). The vertical lines delimit no-flutter regions within the range of investigated $U_{R\alpha}$ (solid-line for Scanlan's model and dashed-line for Theodorsen's model).

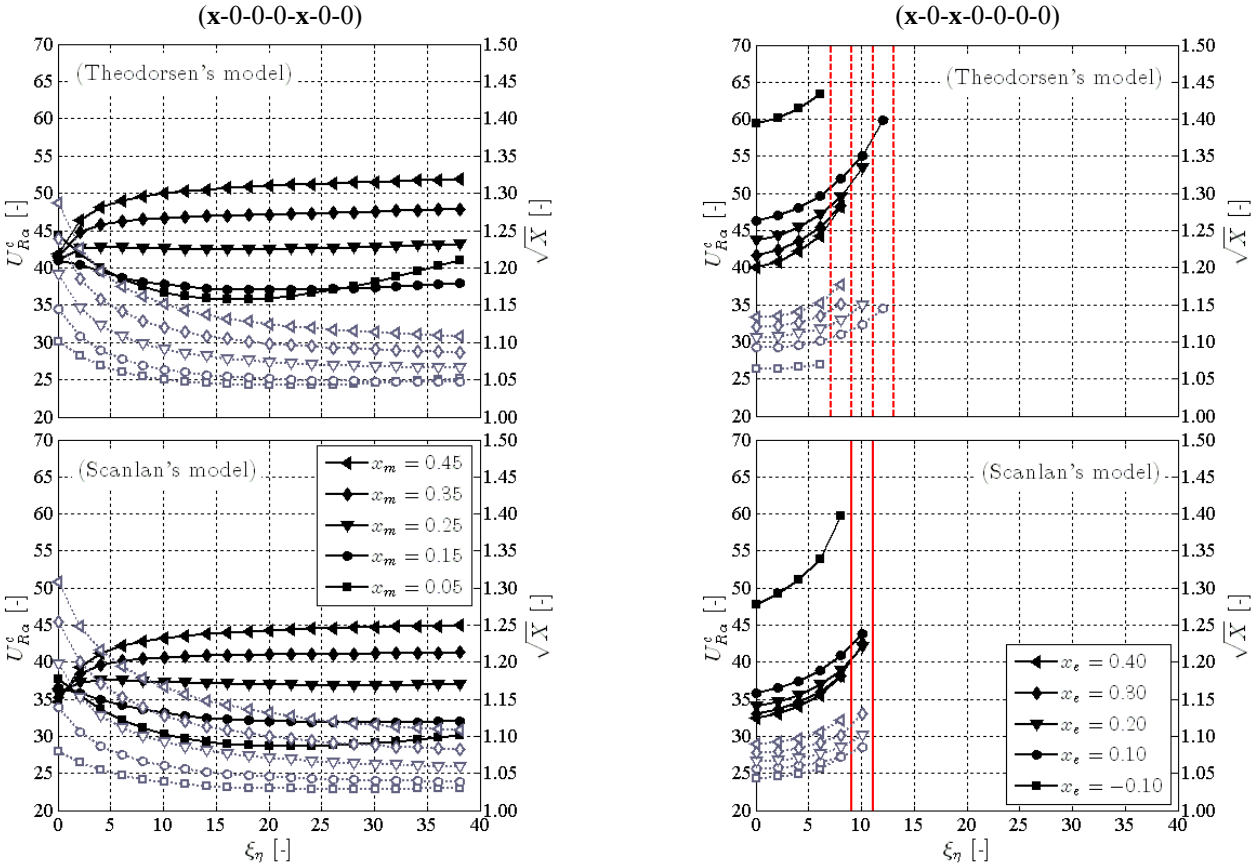

Figure 5. Results of linear analyses obtained varying the heaving damping level and the position of the mass centre (left) or of the elastic centre (right), according to Table 1. Filled markers refer to $U_{R\alpha}$ while empty markers refer to $\sqrt{X}$.

3.2 Experimental LCOs

Wind tunnel tests aimed to experimentally verify the influence of the governing parameters, mainly x_e, x_m and ξ_η, on the instability threshold in terms of critical flow velocity, frequency of oscillation and phase shift. Moreover, attention was paid to explore the post critical behaviour and to investigate the stability features of the observed LCO branches, through the evaluation of the system response to several manually-induced disturbances of different magnitudes.

Figure 6 shows the flutter critical condition estimated via the linear models presented in section 3.1, considering the parameters reported in Table 2. Comparing these results with the experimental ones, a general agreement is found. Nevertheless, the critical velocity of flutter is difficult to be identified experimentally when an hysteresis loop is present in the flutter response and, generally, linear models give results closer to the end of the sub-critical branches.

The experiments confirmed that a significant reduction of the instability threshold is obtained when positive eccentricity of the centre of mass or stiffness is introduced (cases #10 and #21 in Figure 7). In particular for case #21, the slope of the heaving-amplitude vs. reduced-velocity curve is higher than for the other test cases, with relatively moderate pitching amplitudes. For symmetric configurations, the increase of the heaving damping restraints the LCO amplitude in the range immediately beyond the instability onset (Figure 8a) and, according to linear theory, this generally produces a delay of the flutter onset (see section 3.1 and [4]). In case of $x_e > 0$, low damping levels do not considerably affect the critical velocity in agreement to Figure 5 (right-hand side). Moreover, it weakly decreases the slope of both heaving and pitching LCOs and strongly reduces the amplitudes in the subcritical branch (Figure 8b). By contrast, the instability threshold is reduced when $x_m > 0$, according to section 3.1, without affecting the LCO heaving amplitude (Figure 8c). The system seems to be able to compensate the increment of heaving viscous forces increasing the phase shift between the vibration modes and producing larger pitching amplitudes [4]. Skipping of damping levels, from higher values to the pure mechanical one, confirmed the coherence of the results, as it is clear in the left-hand side of Figure 9. The right-hand side of Figure 9 corroborates the results also in terms of build-up, obtained from an imposed rest position at a flow velocity higher than the critical one.

Usually long build-ups were required to reach stable LCO regimes, especially for symmetrical configurations, where neither a stiffness nor a mass eccentricity fosters the instability. Then, the subcritical bifurcation was also observed, showing a stable branch below the critical threshold for decreasing wind speed, in agreement with previous results [39]. This branch is particularly remarkable for configurations with a downstream mass unbalance, as clearly shown in Figure 8c. In this case, the system is able to oscillate down to about $0.85U_c$ (being U_c the critical velocity), featuring a quasi-periodic response (Figure 9).

It has to be remarked that an undesired increase of the pitching mechanical damping was observed for large amplitudes of oscillation, due to the friction between the tensioned cables, used to restrain the sway motion and the supports of the model. Since the instability observed in tests seems to be of pitching-branch type, this effect could have non-negligibly influence on the evolution of the LCO. Consequently, the slope of all the amplitude-velocity curves may have been higher in case of constant pitching damping.

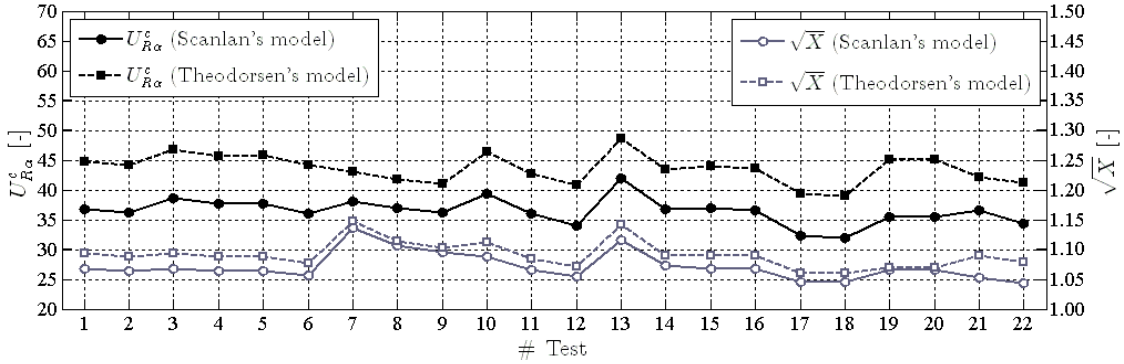

Figure 6. Linear flutter predictions for all the configurations tested during the experimental campaign (see Table 2).

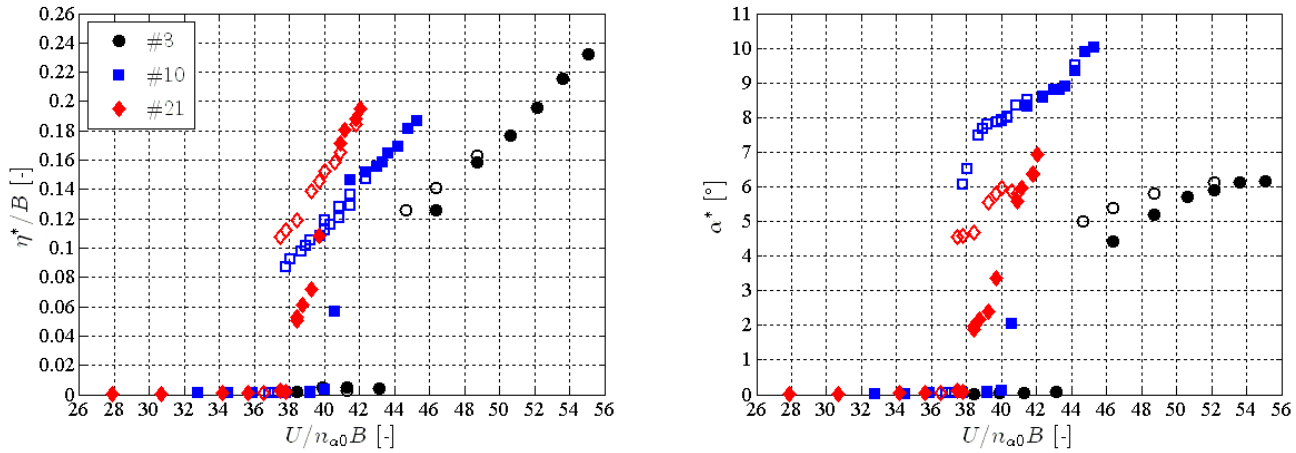

Figure 7. LCOs for some test cases without added damping: symmetrical configuration (#3) and configuration with positive eccentricity of the mass centre (#10) or elastic centre (#21). In the left-hand side is reported the maximum heaving amplitude and in the right-hand side the maximum pitching amplitude, during the steady-state regime. Empty-markers refer to tests with decreasing wind speed.

(a)

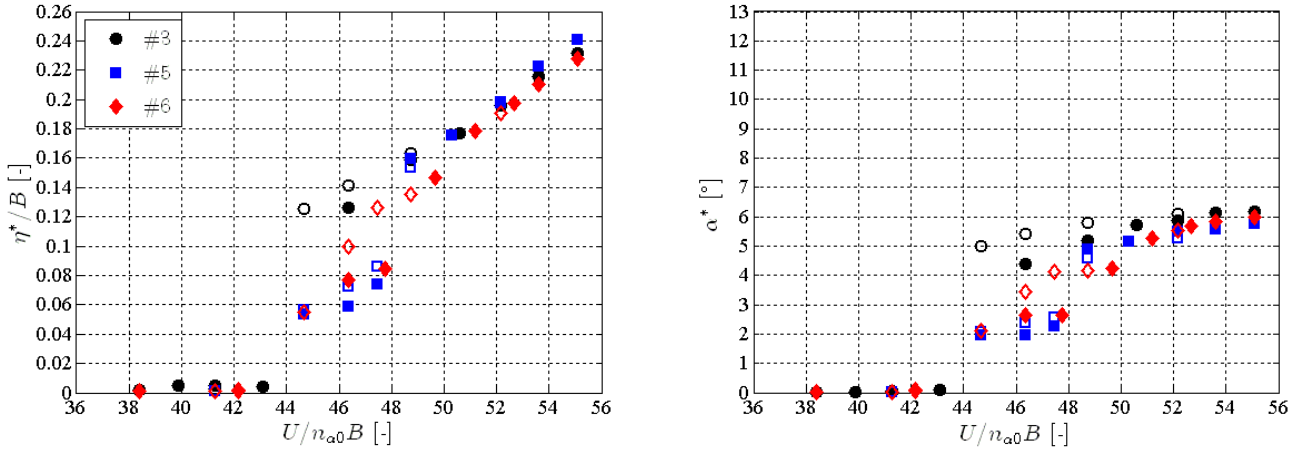

(b)

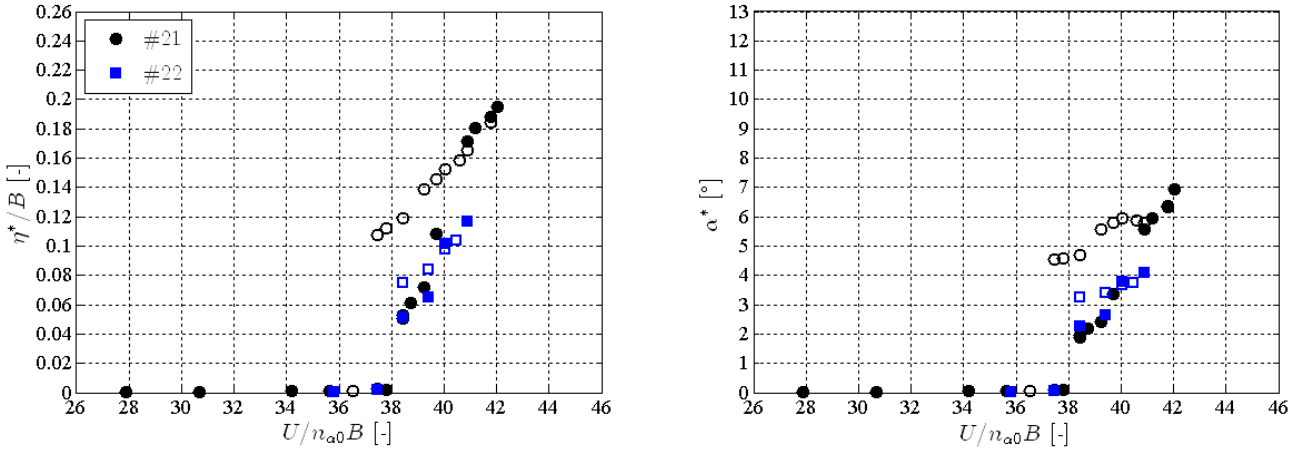

(c)

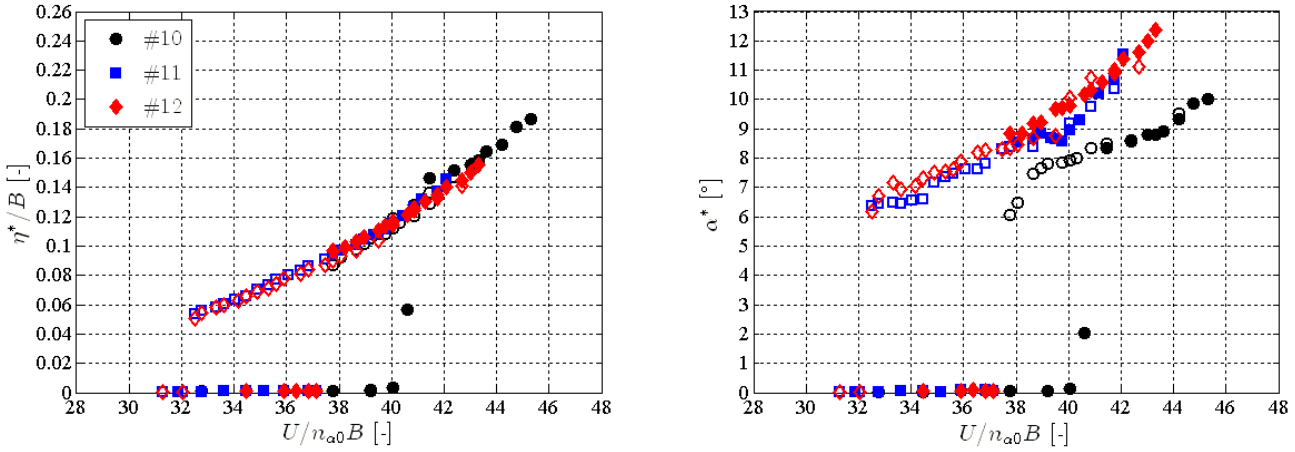

Figure 8. LCO amplitudes for different heaving damping ratios: effects of added heaving damping for symmetrical configurations (a) and on test cases with positive eccentricity of elastic (b) or mass centres (c). In the left-hand side is reported the maximum heaving amplitude and in the right-hand side the maximum pitching amplitude, during the steady-state oscillations. Empty-markers refer to tests with decreasing wind speed.

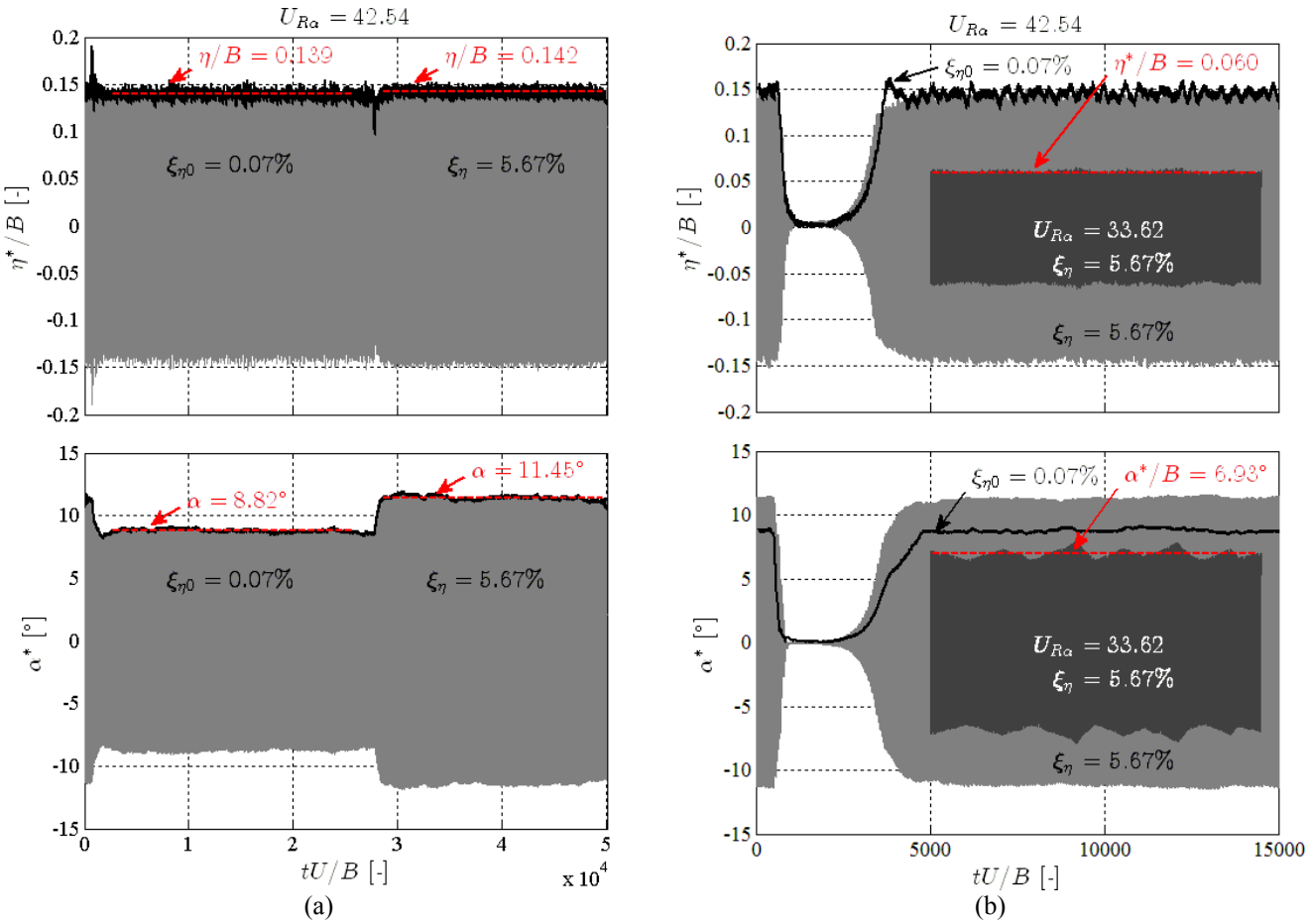

Figure 9. Test case with positive eccentricity of the mass centre: example of a test with a jump in the heaving damping level (a); comparison of build-ups at a post-critical velocity for two damping ratios and time history for a subcritical wind speed (b). Black lines describe the envelope of the motion signal while red-dashed lines indicate the average value of amplitude reached at steady-state oscillations.

3.3 Power efficiency

As a preliminary study on flutter-based energy generators, the efficiency evaluation (in a similar way to conventional wind turbines) can be computed according to:

$$\Gamma_\eta^* = \frac{P_\eta^*}{P_W} = \mu \cdot \left(\frac{2\pi}{U_{R\alpha}}\right)^3 \cdot \left[\left(\frac{\eta^*}{B}\right)^2 \cdot \frac{\xi_\eta}{\gamma_n X} - \frac{\eta^*}{B} \cdot \frac{\sin\phi^*}{2} \cdot \frac{\alpha^* x_m}{X^{3/2}}\right] \Big/ \left[\frac{1}{B/D} + 2\frac{\eta^*}{B} + \sin\alpha^* \cdot |\cos\phi^*|\right] \tag{7}$$

Efficiency, Γ_η^*, is here defined as the ratio of the power extracted by the system, P_η^*, to an ideal available flow power, P_W, that is the power per unit area, $1/2\rho U^3$, times the area swept by the moving system, $(D+2\eta^*+B\sin\alpha^*|\cos\phi^*|)\cdot L$. This efficiency refers to the total power extracted from the fluid-structure system, but, given that $\xi_\eta = \xi_{\eta 0} + \xi_E$ (see §2.1), the available power for electricity generation is the portion proportional to ξ_E only. Therefore, the structural damping $\xi_{\eta 0}$ should be as low as possible in order to limit energy dissipation.

Although the parametric linear analyses, explained in sections 2.1 and 3.1, outlined information about optimal configurations and parameters, these preliminary experiments were designed according to the characteristics of the wind tunnel facility to allow post-critical measurements. Thus, the efficiencies shown in Figure 10 are low due to a not-calibration of the system for power generation purposes, in particular due to high values of the reduced critical wind speed. However, the left-hand side of Figure 5 and Figure 8c clearly suggest the possibility to extract higher levels of energy from heaving vibrations simply increasing the heaving damping. Furthermore, focusing the design on the positions of stiffness and mass centres, as well as on the value of the inertial parameters and ratio of the still-air frequencies, more unstable (then rentable) configurations can be conceived.

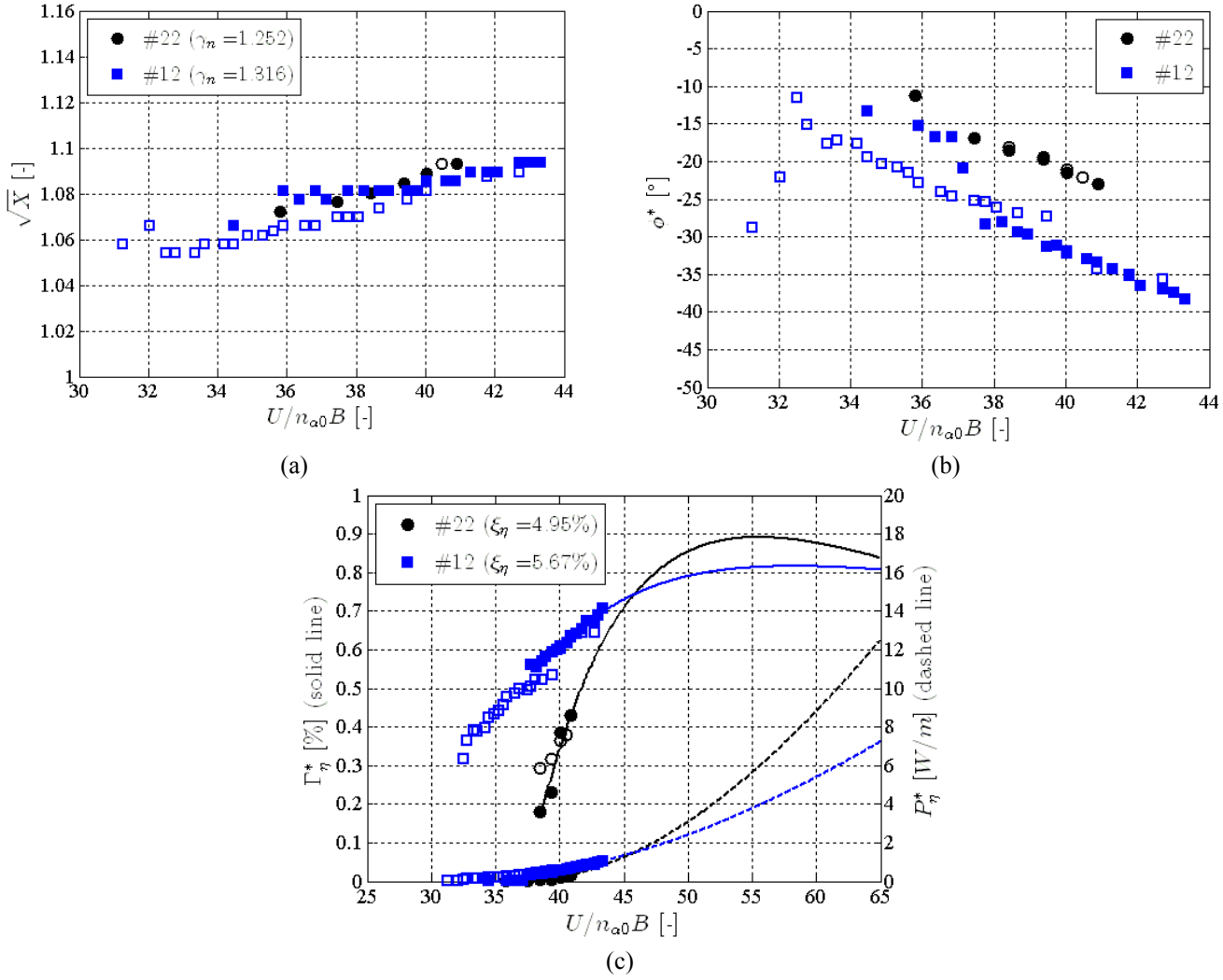

Figure 10. Evolution of nondimensional flutter frequency (a), phase angle (b) and resulting energy performances (c) for the configurations with positive eccentricity of mass and elastic centres. In the latter, the governing parameters are approximated by a linear fitting to extrapolate the power performance at higher reduced velocities.

4 CONCLUSIONS

A systematic theoretical and experimental approach was used to explore the behaviour of a flat plate model with rectangular 15:1 cross section undergoing two-degree-of-freedom classical flutter, for energy harvesting purposes. Linear models were used to investigate the flutter critical condition and the influence of the governing parameters, performing parametric studies in order to find optimal configurations. Wind tunnel aeroelastic tests on a sectional model were conducted to observe the critical and post-critical behaviour for several configurations and to make comparisons with the analytical predictions. The role played by a few key parameters of the system was systematically investigated, shedding light on the flutter phenomenon and preliminarily discussing the energy harvesting performances. For power generation purposes, proper eccentricities of elastic and mass centres downstream the midchord of the cross section can be introduced as tuning solutions for optimal operative ranges. An additional reduction of the critical reduced velocity can be obtained by simply increasing the heaving damping in case of small positive eccentricity of the mass centre.

The next step will be to focus the investigation on the power efficiency instead of the critical reduced velocity and flutter frequency. The goal is to consider the combination of these two parameters directly in the efficiency of the system by Eq. (7), looking for final optimal configurations. Hence, the combination of more effects will be studied to maximize the harnessed energy.

In the future, improvements of the experimental setup are planned, for instance using ball bearings to restrain the sway motion, since the influence of the pitching damping on the subcritical branch of some limit cycles of oscillation still needs to be clarified. Static force coefficients and flutter derivatives measurements will be implemented to supply more information for the analytical modelling. Furthermore, more powerful dampers (or directly an energy conversion apparatus, for example using solenoid-based transducers) can be used to perform tests with very high damping levels.

ACKNOWLEDGMENTS

The authors gratefully acknowledge the contribution of Dr. Hodei Aizpurua Aldaroso during the experimental tests in the Stahlbau Wind Tunnel of TU Braunshcweig and the staff of the Stahlbau laboratory during the model and setup development.

REFERENCES

[1] E. Simiu and R. H. Scanlan, Wind effects on structures: fundamentals and applications to design, 3rd ed., New York: John Wiley and Sons, Inc., 1996.

[2] F. B. Farquharson, F. C. Smith, G. S. Vincent, T. von Kármán and L. G. Dunn, "Aerodynamic stability of suspension bridges with special reference to the tacoma," Bulletin of the Universtity of Washington, Seattle, Washington, 1949-1954.

[3] Y. Fung, An Introduction to the Theory of Aeroelasticity, New York: John Wiley and Scons, Inc., 1955.

[4] R. Bisplinghoff and H. Ashley, Principles of Aeroelasticity, NewYork: John Wiley and Sons, Inc., 1962.

[5] E. Dowell, J. Edwards and T. Strganac, "Nonlinear aeroelasticity," *J. Aircraft,* vol. 40, no. 5, pp. 857-874, 2003.

[6] S. Roundy, "On the effectiveness of vibration-based energy harvesting,," *J. Intel. Mat. Syst. Str.,* vol. 16, no. 10, pp. 809-823, 2005.

[7] M. M. Bernitsas, K. Raghavan, Y. Ben-Simon and E. M. H. Garcia, "VIVACE (Vortex Induced Vibration Aquatic Clean Energy): A New Concept in Generation of Clean and Renewable Energy From Fluid Flow," *J. Offshore Mech. Arct.,* vol. 130, no. 4, pp. 041101 (1-15), 2008.

[8] G. Ahmadi, "An oscillatory wind energy convertor," *Wind Energy,* vol. 18, pp. 115-120, 1978.

[9] A. Barrero-Gil, G. Alonso and A. Sanz-Andres, "Energy harvesting from transverse galloping," *J. Sound Vib.,* vol. 329, no. 14, p. 2873–2883, 2010.

[10] L. Caracoglia, "Feasibility assessment of a leading-edge-flutter wind power generator," *J. Wind Eng. Ind. Aerod.,* vol. 98, no. 10-11, p. 679–686, 2010.

[11] H.-J. Jung and S.-W. Lee, "The experimental validation of a new energy harvesting system based on the wake galloping phenomenon," *Smart Mater. Struct.,* vol. 20, no. 5, pp. 055022 (1-11), 2011.

[12] W. McKinney and J. De Laurier, "The Wingmill: An Oscillating-Wing Windmill," *J. Energy,* vol. 5, no. 2, pp. 106-115, 1981.

[13] K. Jones, S. Davids and M. Platzer, "Oscillating-wing power generation," in *Proc. 3rd ASME/JSME Joint Fluids Engineering Conf.*, 1999.

[14] K. Isogai, M. Yamasaki, M. Matsubara and T. Asaoka, "Design study of elastically supported flapping wing power generator," in *Int. Forum on Aeroelasticity and Structural Dynamics*, Amsterdam, 2003.

[15] B. B. Simpson, F. Hover and M. Triantafyllou, "Experiments in direct energy extraction through flapping foils," in *Proc. 18th Int. Offshore and Polar Engineering Conf.*, Vancouver, Canada, 2008.

[16] Q. Zhu, M. Haase and C. H. Wu, "Modeling the capacity of a novel flow-energy harvester," *Appl. Math. Model.,* vol. 33, no. 5, p. 2207–2217, 2009.

[17] Z. Peng and Q. Zhu, "Energy harvesting through flow-induced oscillations of a foil," *Phys. Fluids,* vol. 21, pp. 123602 (1-9), 2009.

[18] K. Isogai and H. Abiru, "Study of Multi-Wing Configurations of Elastically Supported Flapping Wing Power Generator," *T. Jpn. Soc. Aeronaut. S.,* vol. 55, no. 2, p. 133–142, 2012.

[19] M. Bryant and E. Garcia, "Modeling and Testing of a Novel Aeroelastic Flutter Energy Harvester," *J. Vib. Acoustics,* vol. 133, no. 1, pp. 011010 (1-11), 2011.

[20] J. Allen and A. Smits, "Energy harvesting eel," *J. Fluid. Struct.,* vol. 15, pp. 1-12, 2001.

[21] L. Tang, "The dynamics of two-dimensional cantilevered flexible plates in axial flow and a new energy-harvesting concept," Montréal, Canada, 2007.

[22] F. Fei, J. D. Mai and W. J. Li, "A wind-flutter energy converter for powering wireless sensors," *Sensor. Actuat. A-Phys.,* vol. 173, no. 1, p. 163–171, 2012.

[23] A. Barrero-Gil, S. Pindado and S. Avila, "Extracting energy from Vortex-Induced Vibrations: A parametric study," *Appl. Math. Model.,* vol. 36, no. 7, p. 3153–3160, 2012.

[24] C. Grouthier, S. Michelin and E. De Langre, "Energy harvesting using vortex-induced vibrations of tensioned cables," *arXiv preprint arXiv:1203.0236,* pp. 1-11, 2012.

[25] O. M. S. Doaré, "Piezoelectric coupling in energy-harvesting fluttering flexible plates: linear stability analysis and conversion efficiency," *J. Fluids Struct.,* vol. 27, no. 8, pp. 1-40, 2011.

[26] S. Michelin and O. Doaré, "Energy harvesting efficiency of piezoelectric flags in axial flows," *J. Fluid Mech.,* vol. 714, p. 489–504, 2013.

[27] E. Dowell, R. Clark, D. Cox, H. Curtiss, J. Edwards, D. Peters, R. Scanlan, E. Simiu, F. Sisto, K. Hall and T. W. Strganac, A Modern Course in Aeroelasticity (Solid Mechanics and Its Applications), 4th ed., Klower, USA: Springer, 2004.

[28] S. Bhat and R. Govardhan, "Stall flutter of NACA0012 airfoil at low Reynolds numbers," *J. Fluids Struct.,* vol. 41, p. 166–174, 2013.

[29] W. McCroskey, "Unsteady airfoils," *Annu. Rev. Fluid Mech.,* vol. 14, p. 285–311, 1982.

[30] S. Sarkar and H. Bijl, "Nonlinear aeroelastic behavior of an oscillating airfoil during stall induced vibration," *J. Fluids Struct.,* vol. 24, p. 757–777, 2008.

[31] N. Razak, T. Andrianne and G. Dimitriadis, "Flutter and stall flutter of a rectangular wing in a wind tunnel," *J. AIAA,* vol. 49, no. 10, p. 2258–2271, 2011.

[32] R. H. Scanlan, "Problematics in formulation of wind-force models for bridge decks," *J. Eng. Mech,* vol. 119, no. 7, pp. 1353-1375, 1993.

[33] J. Larsen, S. Nielsen and S. Krenk, "Dynamic stall model for wind turbine airfoils," *J. Fluids Struct.,* vol. 23, pp. 959-982, 2007.

[34] J. Leishman and T. Beddoes, "A semi-empirical model for dynamic stall," *J. Am. Helicopter Soc.,* vol. 34, no. 3, pp. 3-17, 1989.

[35] D. Petot, "Modélisation du décrochage dynamique par équations différentielles," *La Recherche Aérospatiale,* vol. 5, pp. 59-72, 1989.

[36] C. W. Emory, "Prediction of Limit Cycle Oscillation in an Aeroelastic System using Nonlinear Normal Modes," Blacksburg, Virginia, 2010.

[37] A. Abdelkefi, R. Vasconcellos, F. D. Marques and M. R. Hajj, "Modeling and identification of freeplay nonlinearity," *J. Sound Vib.,* vol. 331, no. 8, pp. 1898-1907, 2012.

[38] P. Dunn and J. Dugundji, "Nonlinear stall flutter and divergence analysis of cantilevered graphite/epoxy wings," *J. AIAA,* vol. 30, no. 1, p. 153–162, 1992.

[39] X. Amandolese, S. Michelin and M. Choquel, "Low speed flutter and limit cycle oscillations of a two-degree-of-freedom flat plate in a wind tunnel," *J. Fluid. Struct.,* vol. 43, pp. 244-255, 2013.

[40] M. Matsumoto, "Aerodynamic damping of prisms," *J. Wind. Eng. Ind. Aerod.,* vol. 59, pp. 159-175, 1996.